Arch. Metall. Mater. **70** (2025), 2, 531-538

DOI: https://doi.org/10.24425/amm.2025.153453

XINSHENG WANG[1,2], YANG ZHENG[1,2], GUOYONG YE[1*], ZHIHAN ZHANG[2], KAIXIONG GAO[3], WENJIANG BI[4], YANPEI LIU[5]

EFFECT AND MODELING ANALYSIS OF ADDING CERAMIC POWDER TO THE SURFACE OF GEARS FOR COATING PERFORMANCE

Gear provides an important means of transmission in the automobile, and the service life of the gear teeth has a direct effect on how the engine performs. To enhance the strengthening performance of gear surface, three composite coatings were prepared in this paper by supersonic flame spraying technology, with nickel-based powder as the main material, and ceramic powder WC, TiO_2 and Cr_3C_2 added to it respectively. Hardness tester, scanning electron microscope, X-ray diffractometer and other devices were used to comparatively evaluate the performance of the coatings. Then, static simulation was carried out for the coating. The results show that the coating containing Cr_3C_2 is superior to the other two coatings in densification and hardness. Finally, ANSYS software was applied to model the gear surface coating, revealing that the gear with Cr_3C_2 ceramic powder is advantageous over the coating with TiO_2 particles.

Keywords: Gear; Ceramic particles; Supersonic flame spraying; Simulation

1. Introduce

As the automotive industry advances rapidly, the role of gears in automotive transmission systems has become increasingly prominent. Nowadays, they are widely used in a range of civil and military equipment, such as metallurgical machinery, heavy vehicles, ship machinery, aerospace machinery, etc. [1-4]. In general, most mechanical transmission systems operate under harsh operating conditions characterized by heavy loads, high temperatures. In this circumstance, the gears are susceptible to friction and wear during the meshing process, which results in surface damage [5-10], as shown in Fig. 1. Ultimately, the performance of the gears deteriorates, which reduces the performance of the entire mechanical transmission system. Overall, the failure rate of gears is high, as are their costs. Once they fail and get discarded, considerable resources are wasted. Thus, it is desirable to extend their service life by repairing the surfaces of failed gears or improving the mechanical properties of surface coatings for the gears. This is crucial for resource conservation, equipment operation safety, and other aspects [11].

In practice, gears can be overloaded and used at high speeds. Meanwhile, they are expected to be smaller, lighter and more durable [12-15]. The advancement of gear theory and manufacturing technology could facilitate in-depth research on the mechanism of gear tooth damage, which is crucial for developing reliable strength calculation methods and improving the bearing capacity of gears [16-18]. In theory, extending the lifespan of gears is inseparable from the development of new tooth profiles represented by point line spray gears. The bearing capacity of gears can be improved by developing new tooth teaching materials and new manufacturing processes for gears, exploring the elastic deformation, manufacturing and installation errors, and temperature field distribution of gears, carrying out gear tooth modification to ensure the smooth operation of cargo ships, and increasing the contact area between the wheels and cargo at full load [19].

For the extended lifespan of gears, coating technology has been widely applied to protect the surface of automotive gears. Compared with traditional coating materials, the spray coatings obtained from ceramic powders have attracted much more at-

[1] ZHENGZHOU UNIVERSITY OF LIGHT INDUSTRY, HENNAN KEY LABORATORY OF INTELLIGENT MANUFACTURING OF MECHANICAL EQUIPMENT, ZHENGZHOU, 430002, CHINA
[2] ZHENGZHOU UNIVERSITY OF LIGHT INDUSTRY, MECHANICAL AND ELECTRICAL ENGINEERING INSTITUTE, ZHENGZHOU, 430002, CHINA
[3] CHINESE ACADEMY OF SCIENCES, LANZHOU INSTITUTE OF CHEMICAL PHYSICS 730000 LANZHOU, CHINA
[4] HENAN DBOE CO., LTD, NANYANG, HENAN PROVINCE, 473000, CHINA
[5] ZHENGZHOU UNIVERSITY OF LIGHT INDUSTRY, SCHOOL OF COMPUTER SCIENCE AND TECHNOLOGY, ZHENGZHOU, 430002, CHINA

* Corresponding author: guoyongye2021@163.com

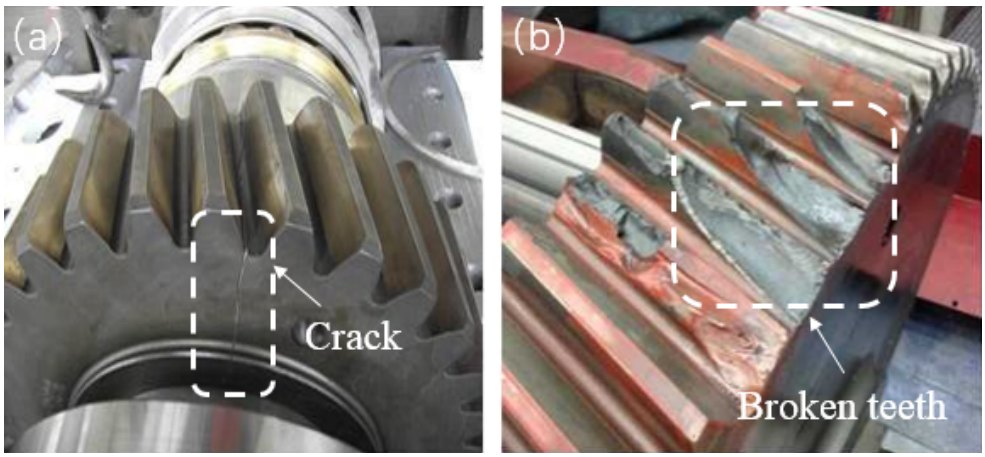

Fig. 1. Common failure modes of gears, (a) Crack, (b) Broken teeth

tention for their excellent properties such as high hardness, high wear resistance, and high corrosion resistance.

Developed by Browning Company in the 1980s, the supersonic flame spraying technology is effective in preventing oxidation and degradation for coatings. It is particularly suitable for spraying powders mainly composed of carbides. Among the surface technology methods, plasma spraying is one of the common surface modification and strengthening technology, which makes the metal surface possess the properties of wear-resistance, high temperature oxidation, corrosion resistance, electrical insulation and radiation protection. Currently, it has been widely applied in many sectors such as gear machinery, aerospace engines, aircraft landing gear, etc. [20-21]. Marx et al. conducted a study to demonstrate that flame spraying with low temperature and speed can lead to higher porosity, while the porosity of supersonic flame spraying coatings could reach as low as 0.5% or less [22-23]. Zhao et al. established a multiphase coupling numerical model of HVOF thermal spraying, calculated the compressible turbulence and combustion behavior during the thermal spraying in the transient state, and quantitatively explored the time-varying evolution mechanism of the multiphase flow formed by the particles wrapped with the combustion flame flow [24]. Therefore, the High Velocity Oxygen Fuel (HVOF) process is currently one of the important technical means used to prepare the coatings containing WC, TiO_2, and Cr_3C_2 [25-29]. The HV-8000 model is a representative of the existing supersonic flame spraying system. Compared with previous supersonic flame spraying equipment, it possesses various advantages. On the one hand, it addresses low equipment power and low particle speed, which extends the heating time of powder particles in the flame. On the other hand, its spraying powder is supplied via a central axis, which allows the powder to stay in the flame longer. Thus, it can be uniformly heated and melted to produce a concentrated spray beam, with a significant improvement in the particle flight speed [30]. Ultimately, the quality of the coating produced is significantly improved.

In this paper, the HV-8000 supersonic flame spraying system is applied to prepare WC, TiO_2, Cr_3C_2 reinforced Ni60+Ni (MoS_2) coatings, for an investigation into the effects of three different reinforcement particles on structure and mechanical properties of the coating.

2. Experiments

2.1. Preparation method

The substrate material selected for experimental purpose is 45# steel plate with the dimensions of Φ30 × 10 mm. After being ground to remove rust from the surface, it was subjected to shot peening for enhancement treatment. Then, it was cleaned with acetone to maintain surface cleanliness. Fig. 2 shows the schematic diagram of coating preparation. In the selection of coating materials, the main component is Ni based powder with excellent mechanical properties. The coating made from this powder performs well in wear resistance, hardness, toughness, impact resistance and oxidation resistance, with a low cost incurred. Ni60 powder possesses a spherical structure with a high degree of spheroidization, and the powder has a diameter in the range of 50-80 μm. Ni (MoS_2) powder is a core-shell composite material, representing a novel type of composite material developed in recent years, which is composed of core particles and surface layer. The surface layer is composed of Ni elements, with MoS_2 as the core particles. WC powder particles are spherical particles with slight pits on the surface, exhibiting a honeycomb shape. The powder dispersion is satisfactory, and the diameter is slightly smaller compared to nickel- based powder particles, ranging from 30-50 μm. The particles of TiO_2 powder are flocculent, and there are polygonal particles in the Cr_3C_2 powder. The powder ratio of the coating is shown in TABLE 1. The well-proportioned powder was placed in a planetary ball mill and then ball milled for 2 hours at a speed of 200 r/min. Subsequently, the composite powder was dried in an oven at 120°C for 2 hours to remove moisture. This experiment was performed using the HV-8000 supersonic flame spraying equipment to prepare composite coatings. The spraying distance was set to 120 mm and the maximum flame temperature was set to 3000°C. The process parameters are detailed in TABLE 2.

TABLE 1

Powder ratio of composite coating

Sample number	Powder ratio
A	Ni60+35 wt%Ni(MoS_2)+15 wt%WC
B	Ni60+35 wt%Ni(MoS_2)+15 wt%TiO_2
C	Ni60+35 wt%Ni(MoS_2)+15 wt%Cr_3C_2

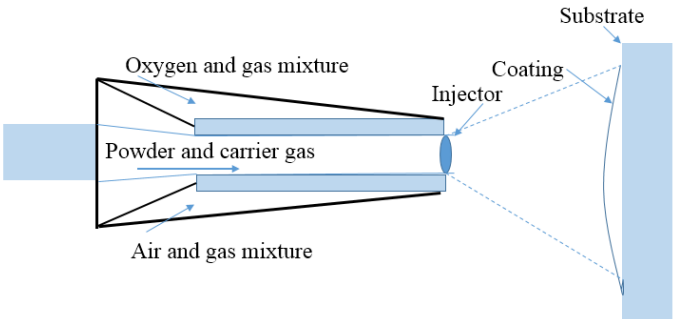

Fig. 2. Schematic diagram of Coating

2.2. Testing and Performance Characterization

The composition of the coating phases was examined with Japanese Shimadzu X-ray diffractometer (model: XRD-7000) for a Cu target, with the scanning angle set to 10-80° and the scanning speed set to 8°/min. The field emission scanning electron microscope (SEM, model: JEM-1200EX) produced in the Czech Republic was used to examine the surface and cross-sectional microstructure of the coating. A Rockwell hardness tester was used to determine the hardness values in the upper, middle, and lower areas of the coating by applying a load of 150 kg for 10 seconds.

3. Results and discussion

3.1. Phase analysis

Fig. 3 shows the results of phase analysis conducted by using an X-ray diffractometer on three different composite coatings. The main phases of the three coatings may be composed of Ni, MoB, and Cr_3Ni_2Si phases, with the highest peak value shown by the Ni phase. The appearance of MoB phase peak value is potentially attributed to the intervention of various impurities such as dust and particles during the spraying process. Also, Mo reacts with a small amount of B element in nickel-based powder due to the high temperature of flame spraying. The reaction between Ni element and Si element in Cr and nickel-based powder is possibly one of the factors contributing to the appearance of Cr_3Ni_2Si phase. In the coating, the content of TiO_2 and WC particles is low, it is not appeared TiO_2, WC, and W_2C phase peaks were detected in the coating.

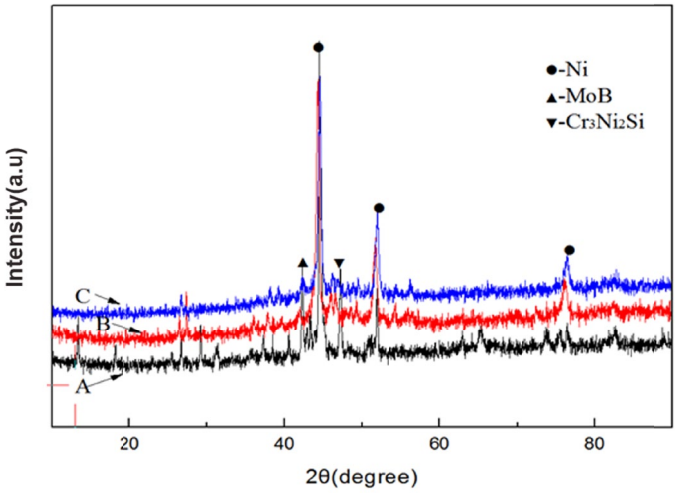

Fig. 3. Results of coating phase analysis

3.2. Microscopic morphology analysis of coatings

3.2.1. Microscopic morphology of coating surface

Fig. 4 shows the images of three coatings as captured through scanning electron microscopy at 500×, 1000×, and 5000× magnifications. According to Fig. 4(a), the adhesion between powder particles is tight and the distribution is relatively uniform, with the layered structure found more pronounced than nickel-based powder. Fig. 4(b) shows that there remain some circular unmelted particles on the surface of the coating. As can be seen clearly from Fig. 4(c), the overall density of the coating is high, despite a few pores remaining on the surface, and the porosity of the coating is uneven. In Figs. 4(d-f), pores and non-melted powder particles remain in the coating sprayed with TiO_2 particles. The surface density of its coating is low, cracks exist, and high-temperature oxides are formed. As shown in Figs. 4(h, i, g), the coating added with Cr_3C_2 powder particles has high density, and the coating possesses a layered structure with non-melted powder particles and pores.

The presence of unmelted particles and pores in all three coatings results mainly from the application of thermal spraying technology. Due to the uneven heating or insufficient heating temperature during spraying, there may be non-melted materials.

TABLE 2

Spraying process parameters

	Spray current (A)	Spray voltage (V)	Argon gas flow rate (m^3/h)	Hydrogen flow rate (m^3/h)	Nitrogen flow rate (m^3/h)	Powder delivery speed (g/min)
Process parameters	360	120	3.6	0.25	0.6	35

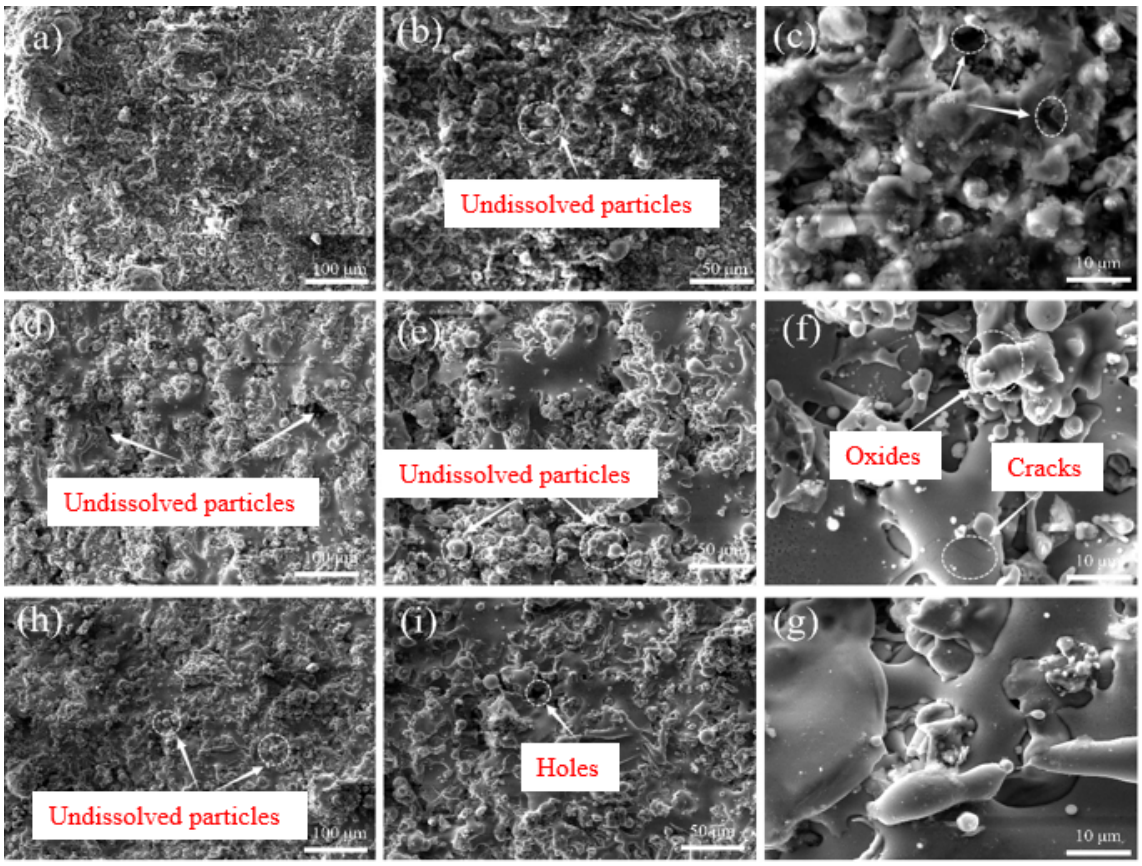

Fig. 4. Cross-sectional morphology of the three coatings; (a-c) Cross section of coating A; (d-f) Cross section of coating B; (h-g) Cross section of coating C

The appearance of pores and voids is attributed to the uneven melting of the sprayed powder, the uneven diffusion of spray gun pressure, and the presence of gas hindering the bonding of a small amount of sprayed material during the spraying process.

The Property of the coating added with TiO_2 powder particles is not as excellent as that of added with WC powder and Cr_3C_2 powder. Besides, there are obvious cracks. However, the uniformity of the coating is improved, and the surface of the coating added with WC is dense. The porosity and surface roughness of the coating added with Cr_3C_2 are slightly higher compared to the other two powder particles, with no obvious cracks present in the coating.

3.2.2. Analysis of cross-sectional morphology in the coating

Figs. 5(a-c) show the cross-sectional microstructure of coatings A, B, and C, respectively, with (c-f) illustrating the enlarged local images. From Fig. 5(a), it can be seen that coating A fails to completely cover the surface of the substrate, with weak adhesion between the substrate and the coating. There remains a large gap, which may cause the coating to peel off in later use, leading to performance failure of the parts. In addition, there are two obvious pores in the coating, with a diameter of 70 μm for pore 1 μm and a diameter of 100 μm for pore 2 μm. This can also lead to low density of the coating. The development of pores may result from the uneven diffusion of spray gun pressure and the gas hindering the bonding of a small amount of sprayed material during the spraying process. Also, there are non-melted powder particles around the pores. A possible reason for this finding is that some powder particles are not uniformly heated, or the heating temperature does not meet the requirements during the spraying process.

Compared to coating B, the adhesion of coating A is slightly tighter. However, there are also some areas between coating B and the substrate that are not covered by the coating, with a small amount of coating being found in the substrate. This may result from the melting of the substrate surface, induced by the high flame temperature during the spraying process, which causes some coatings to penetrate into the substrate. As revealed clearly by magnification, there are also pores and cracks in the coating.

There are still pores between coating C and the substrate. However, compared to the other two composite coatings, this coating is superior in the adhesion between these three coatings and the substrate, with no microcracks formed on its surface. By examining the enlarged cross-sectional morphology, it can be found out that there are very few pores in this coating, indicating its high density.

Through a comparative analysis of the cross-sectional morphology and microstructure among the three different composite coatings, it can be discovered that the coating with Cr_3C_2

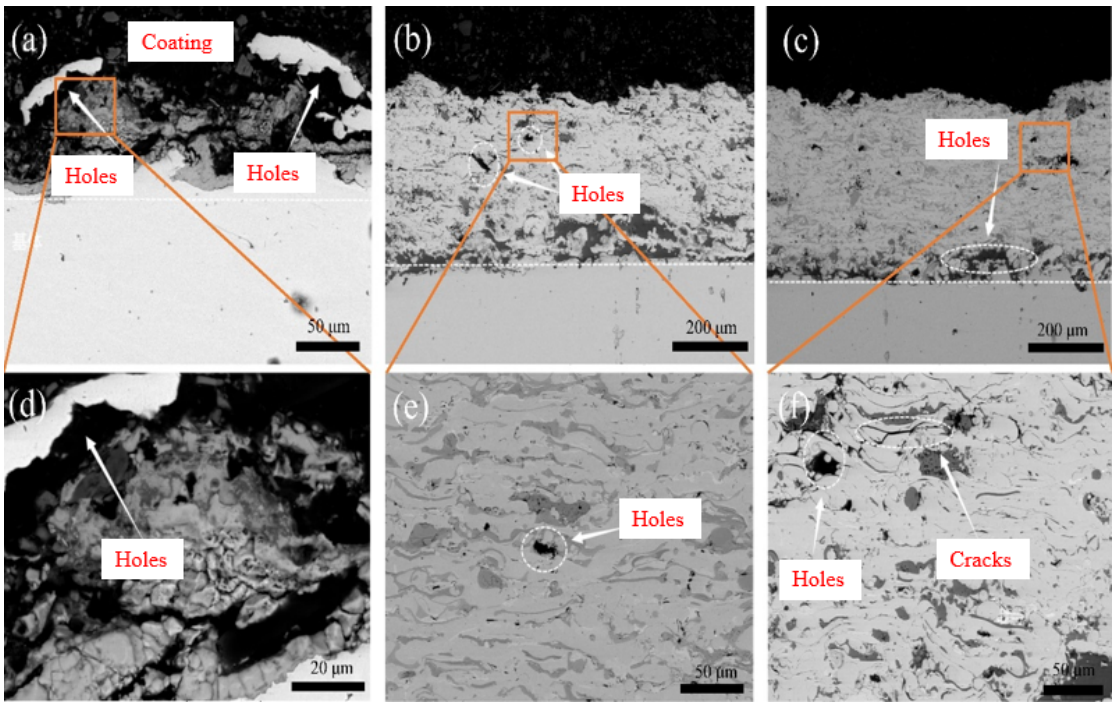

Fig.5. Cross-sectional morphology and local magnification of the three coatings; (a-c) Cross-sectional morphology of coatings A, B and C; (d-f) Partial magnification of the coating

powder performs best in adhesion rate, adhesion, density, and other properties, followed by the coating with TiO_2 powder that exhibits the highest adhesion strength. Conversely, the coating added with WC performs worst in adhesion strength.

3.3. Hardness analysis

Fig. 6 shows the cross-sectional hardness distribution of these three coatings. The average Rockwell hardness values are 72.57 HRC, 73.10 HRC and 74.50 HRC for coatings A, B and C, respectively. The overall hardness of coating C is higher compared to the other two, but the hardness distribution is uniform.

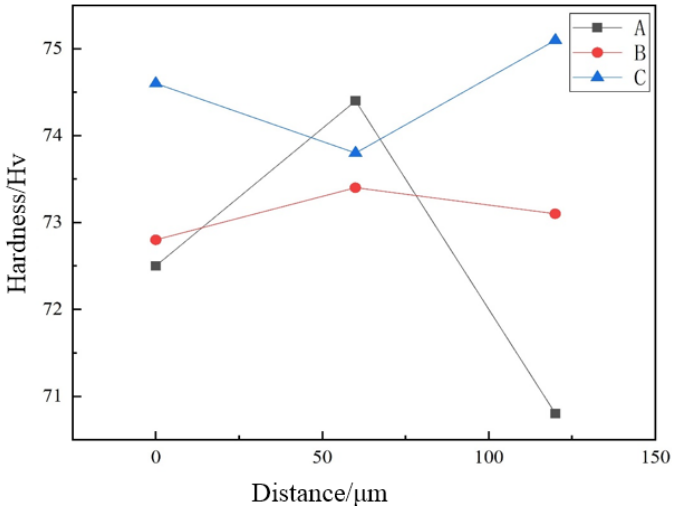

Fig. 6. Distribution of coating hardness with distance

The microhardness of coating C is the highest for two reasons. On the one hand, the crystal structure of Cr_3C_2 particles is rhombic, which leads to high hardness and effectively increases the hardness of the coating. On the other hand, the addition of Cr_3C_2 promotes an increase in the density of the coating.

4. Simulation analysis

4.1. Model establishment

A tooth profile was established above a circle with a diameter of 46 mm such that the contact points between the tooth profile and the circle forms a 10° angle. By drawing a concentric circle with a diameter of 20 mm inside the large circle to serve as the inner ring gear, the surface of the circle was evenly divided into 18 tooth profiles, with a gear thickness of 10 mm. Then, a sketch was drawn, as shown in Fig. 7. The material properties of the gear are defined as 45 steel. According to the previous analysis, the performance of coating added with WC is poor. Therefore, the simulation focuses on the coating added with TiO_2 and Cr_3C_2. The material properties of the coating are detailed in TABLE 3, with the coating thickness set to 1 mm.

TABLE 3

Properties of coating materials

Coatings	Poisson's ratio	Young's modulus (GPa)	Density (g/cm^3)	Temperature (°C)
B	0.27	230	4.23	18
C	0.23	610	6.68	18

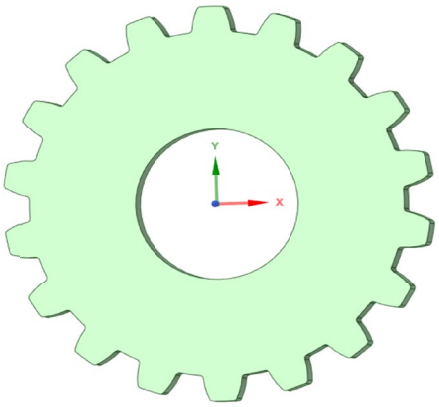

Fig. 7. Gear model

4.2. Static analysis

To perform static structural analysis on the gear tooth profile after meshing, a vertical force of 100 N was applied from top to bottom on the surface of the tooth profile, with the gear ring surface fixed for total deformation calculation. The calculation results are shown in Fig. 8. It can be seen from the figure that the tooth profile undergoes deformation under pressure. There are variations in the severity of bending deformation, with the maximum extent of deformation found at the tooth end. The deformation of the gear tooth profile with coating protection is less severe compared to that without added powder, indicating that the tooth profile with coating protection has a higher

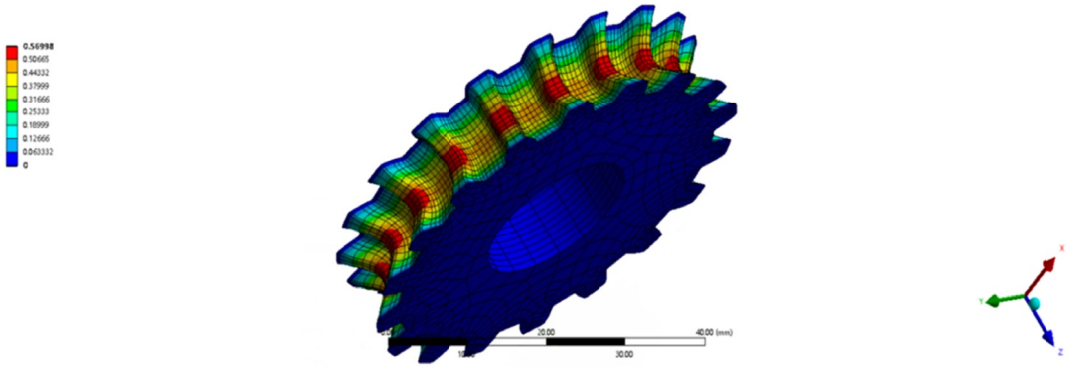

(a) Results of tooth profile equivalent stress calculation

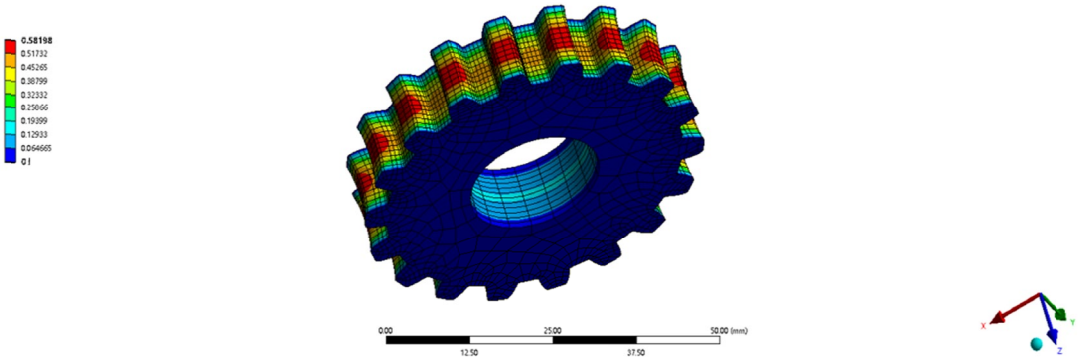

(b) Calculation results of tooth profile equivalent stress after the addition of TiO_2 ceramic powder

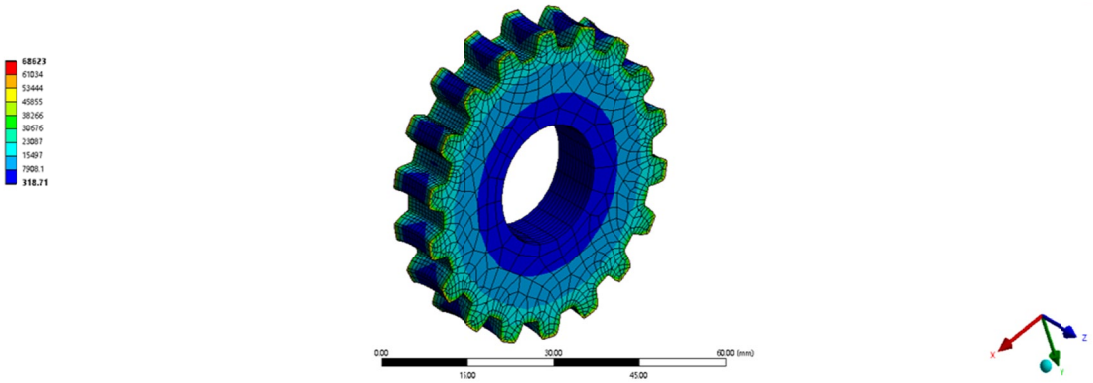

(c) Calculation results of tooth profile equivalent stress after the addition of Cr3C2 ceramic powder

Fig. 8. Cloud image of gear deformation

surface hardness and can withstand greater working pressure. Furthermore, the coating added with Cr_3C_2 powder exhibits less severe deformation than that added with TiO_2 powder, suggesting a better performance of the coating added with Cr_3C_2 powder.

5. Conclusion

This paper investigates the performance of three particle-reinforced coatings, namely WC, TiO_2, and Cr_3C_2, added with Ni60+Ni (MoS_2) powder. The experimental results are consistent with the simulation results. Through simulation analysis, it provides a reference for improving the performance of automotive gears in withstanding deformation. The conclusions are drawn as follows:

(1) The uniformity of the coating added with ceramic powder is improved, with the porosity and surface roughness of the coating containing Cr_3C_2 being slightly higher compared to the other two composite coatings. The addition of WC and Cr_3C_2 powder particles improves the density of the coating, with no cracks present.

(2) The hardness of the coating prepared by adding Cr_3C_2 particles to Ni60+Ni (MoS_2) powder is higher than that of WC and TiO_2 coatings.

(3) According to the static simulation analysis, the Ni60+Ni (MoS_2)+Cr_3C_2 coating performs best in withstanding deformation.

Plasma spraying technology is also constantly innovating and developing with the continuous advancement of science and technology. The emergence of new materials and processes has significantly improved the efficiency and performance of plasma spraying. Meanwhile, the combination with other technologies, such as plasma spraying and 3D printing, provides more possibilities for surface treatment of complex shaped parts. These technological innovations will further broaden the application areas and enhance market prospects of plasma spraying technology.

Acknowledgments

This work is financially supported by the National Science Foundation of China (52475224), Key Scientific and Technological Project of Henan Province (242102240128, 242102211091), Henan Province Science and Technology Research and Development Joint Fund (235200810003,), and Equipment pre research shared technology (50923060203). The authors thank the editor and the anonymous reviewers for their helpful comments and suggestions.

REFERENCES

[1] Haidong Xie, Haowei Yao, Liang Zhang, Research on Powder Metallurgy Gear Lifting Fire Tanker Performance. Procedia Engineering **52**, 453-457 (2013).

[2] Vivek Srivastava, Deependra Singh, A.G. Rao, V.P. Deshmukh, Root cause analysis of flywheel gear failure in a marine diesel engine. Engineering Failure Analysis **156**, 107729-107251 (2024).

[3] Tianli Xie, Jibin Hu, Zengxiong Peng, Chunwang Liu, Synthesis of seven-speed planetary gear trains for heavy-duty commercial vehicle. Mechanism and Machine Theory **90**, 230-239 (2015).

[4] Milan Stanojević, Radoslav Tomović, Lozica Ivanović, Blaža Stojanović, Critical Analysis of Design of Ravigneaux Planetary Gear Trains. Applied Engineering Letters **7** (1), 32-44 (2022).

[5] Min Zhou, Ke Wang, Yang Wang, Kaijia Luo, Hongyong Fu, Liang Si, Online condition diagnosis for a two-stage gearbox machinery of an aerospace utilization system using an ensemble multi-fault features indexing approach. Chinese Journal of Aeronautics **32** (5), 1100-1110 (2019).

[6] Zehua Lu, Dong Wei, Peitang Wei, Huaiju Liu, Huan Yan, Shuixin Yu, Guanyu Deng, Contact fatigue performance and failure mechanisms of Fe-based small-module gears fabricated using powder metallurgy technique. Journal of Materials Research and Technology **26**, 1412-1427 (2023).

[7] Tong Hao Jiang, Zhen Guo Yang, Failure analysis on abnormal cracking of the main landing gear door of a civil aircraft. Engineering Failure Analysis **160**, 108233-10853 (2024).

[8] Dongy Zhang, Xiaoyu Suo, JinYuan Liu, Zhongwei Li, Yanchao Zhang, Hongxing Wu, Study on tribological performances of in situ-boriding laser cladding FeCoCrNiMn layers and its implementation in gear repair. Tribology International **194**, 109503-109515 (2024).

[9] Peng Dai, Jue Lu, Xingyu Liang, Jianping Wang, Fengtao Wang, Dynamic behavior analysis for cages in gear-bearing system with spalling failure on tooth surface. Engineering Failure Analysis **154**, 107657-107678 (2023).

[10] Myron Chernets, Serge Shil'ko, Anatolii Kornienko. Calculated Assessment of Contact Strength, Wear and Resource of Metal-Polymer Gears Made of Dispersion-Reinforced Composites. Applied Engineering Letters **6** (2), 54-61 (2021).

[11] Haifeng He, Heli Liu, Quan Wu, Huawei Chen, A unified model for bending fatigue life prediction of surface-hardened gears, Engineering Failure Analysis **157**, 107964-107981 (2024).

[12] Xin Li, Wen Shao, Jinyuan Tang, Han Ding, Shengyu You, Jiuyue Zhao, Jiling Chen, Numerical modeling and experimental investigation on fatigue failure and contact fatigue life forecasting for 8620H gear. Engineering Fracture Mechanics **296**, 109861-109880 (2024).

[13] Zhou Chen, Yibo Jiang, Sheng Li, Zheming Tong, Shuiguang Tong, Ning Tang, Uncertainty propagation of correlated lubricant properties in gear tribodynamic system. Tribology International **179**, 107812-107828 (2023).

[14] Wenbo Wang, Qiang Guo, Zhibo Yang, Yan Jiang, Jinting Xu, A state-of-the-art review on robotic milling of complex parts with high efficiency and precision. Robotics and Computer-Integrated Manufacturing **79**, 102436-102471 (2023).

[15] Yuhanes Dedy Setiawan Liauw, Mehdi Roozegar, Ting Zou, Alexei Morozov, Jorge Angeles, A topology-change model of multi-speed transmissions in electric vehicles during gear-shifting. Mechatronics **55**, 151-161 (2018).

[16] R. Mohsenzadeh, B.H. Soudmand, K. Shelesh-Nezhad, Load-bearing analysis of polymer nanocomposite gears using a temperature-based step loading technique: Experimental and numerical study. Wear **514-515**, 204595-204617 (2023).

[17] Teruie Takemasu, Takao Koide, Toshinaka Shinbutsu, Hiroshi Sasaki, Yoshinobu Takeda, Satoshi Nishida, Effect of Surface Rolling on Load Bearing Capacity of Pre-alloyed Sintered Steel Gears with Different Densities. Procedia Engineering **81**, 334-339 (2014).

[18] Cheng Wang, Three-dimensional modification for vibration reduction and uniform load distribution focused on unique transmission characteristics of herringbone gear pairs. Mechanical Systems and Signal Processing **210**, 111153-111173 (2024).

[19] Chunpeng Zhang, Jing Wei, Rui Niu, Shaoshuai Hou, Shijie Zhang, Similarity and experimental prediction on load sharing performance of planetary gear transmission system. Mechanism and Machine Theory **180**, 105163-105179 (2023).

[20] Igor Kravchenko, Yury Kuznetsov, Julia Velichko, Svetlana Yarina, Aleksey Dobychin, Dejan Spasić, Larisa Kalashnikova, Model for Evaluating the Plasma Coating Method. Advanced Engineering Letters **2** (1), 21-27 (2023).

[21] Zachary Monette, Ashish K. Kasar, M. Daroonparvar , Pradeep L. Menezes, Supersonic particle deposition as an additive technology: methods, challenges, and applications. The International Journal of Advanced Manufacturing Technology **106**, 2079-2099 (2020).

[22] O. Rojas, R. Muñoz, J.D. Holguín, M.E. López, H. Ageorges, F. Vargas, Porosity formation phenomena in glass particles atomised by oxyacetylene flame-spraying: Effect of feedstock powders and atomisation conditions. Ceramics International **49** (9), 14512-14524 (2023).

[23] YanXin Dan, XiaoMei Liu, Yu Wang, Jing Huang, Hidetoshi Saitoh, Yi Liu, Hua Li, Investigation of the morphologies of chelate flame-sprayed metal oxide splats. Surface and Coatings Technology **460**, 129432-129443 (2023).

[24] Xiaoyu Zhao, Chang Li, Siyu Li, Haisheng Jiang, Xing Han, Time-varying evolutionary mechanism analysis of the multiphase flow during high-velocity oxygen-fuel (HVOF) thermal spraying WC-12Co particle. Surface Coatings Technology **461**, 129435 (2023).

[25] Raunak Supekar, Rakesh Bhaskaran Nair, André McDonald, Pantcho Stoyanov, Sliding wear behavior of high entropy alloy coatings deposited through cold spraying and flame spraying: A comparative assessment. Wear **516-517**, 204596-204608 (2023).

[26] H. Myalska-Głowacka, G. Bolelli, L. Lusvarghi, G. Cios, M. Godzierz, V. Talaniuk, Influence of nano-sized WC addition on the microstructure, residual stress, and tribological properties of WC-Co HVAF-sprayed coatings. Surface and Coatings Technology **482**, 130696-13109 (2024).

[27] Nenad Radić, Mila Ilić, Stevan Stojadinović, Jelena Milić, Jelena Avdalović, Zoran Šaponjić, Photocatalytically active Ag-doped TiO2 coatings developed by plasma electrolytic oxidation in the presence of colloidal Ag nanoparticles. Journal of Physics and Chemistry of Solids **188**, 111918-111926 (2024).

[28] Dehui Ji, Huizhuang, Qiang Hu, Hailong Yao, Youliang Zhang, Hui Guo, Huoping Zhao, Mingxue Shen, Effect of abrasive particle size on the tribological behavior of thermal sprayed WC-Cr3C2-Ni coatings. Journal of Alloys and Compounds **924**, 166536-166549 (2022).

[29] Milan Bukvić, Sandra Gajević, Aleksandar Skulić, Slobodan Savić, Aleksandar Ašonja, Blaža Stojanović, Tribological Application of Nanocomposite Additives in Industrial Oils. Lubricants **12**, 1-6 (2023).

[30] Xinsheng Wang, Jifeng Luo, Yang Li, Honglin Mou, Zhiguo Xing, Zhihai Cai, Shizhong Wei, Yueyang Yu, Properties of laser cladding $(NiCoCr)_{94}Al_3Ti_3$-cBN-hBN hard self-lubricating Ceramic coating. Ceramics International **50** (8), 13761-13769 (2024).